Dynamical magnetic susceptibility in the lamellar cobaltate superconductor $Na_xCoO_2{\cdot}yH_2O$

M.M. Korshunov [1,2*] and I. Eremin [1,3]
[1] *Max-Planck-Institut für Physik komplexer Systeme, D-01187 Dresden, Germany*
[2] *L.V. Kirensky Institute of Physics, Siberian Branch of Russian Academy of Sciences, 660036 Krasnoyarsk, Russia and*
[3] *Institute für Mathematische und Theoretische Physik, TU Braunschweig, 38106 Braunschweig, Germany*
(Dated: August 18, 2007)

We systematically analyze the influence of the superconducting gap symmetry and the electronic structure on the dynamical spin susceptibility in superconducting $Na_xCoO_2{\cdot}yH_2O$ within a three different models: the single a_{1g}-band model with nearest-neighbor hoppings, the realistic three-band t_{2g}-model with, and without e'_g pockets present at the Fermi surface. We show that the magnetic response in the normal state is dominated by the incommensurate antiferromagnetic spin density wave fluctuations at large momenta in agreement with experimental temperature dependence of the spin-lattice relaxation rate. Also, we demonstrate that the presence or the absence of the e'_g-pockets at the Fermi surface does not affect significantly this conclusion. In the superconducting state our results for $d_{x^2-y^2}$- or d_{xy}-wave symmetries of the superconducting order parameter are consistent with experimental data and exclude nodeless $d_{x^2-y^2}+id_{xy}$-wave symmetry. We further point out that the spin-resonance peak proposed earlier is improbable for the realistic band structure of $Na_xCoO_2{\cdot}yH_2O$. Moreover, even if present the resonance peak is confined to the antiferromagnetic wave vector and disappears away from it.

PACS numbers: 74.70.-b; 75.40.Gb; 74.20.Rp; 74.25.Jb

I. INTRODUCTION

The spin dynamics in unconventional non s-wave superconductors is of fundamental interest due to its interesting and peculiar properties. This includes a non-trivial behavior of the magnetic part of the Knight shift in the spin-triplet superconductors[1], as well as an emergence of the so-called resonance peak observed in superconducting layered cuprates[2] which possesses spin-singlet $d_{x^2-y^2}$-wave order parameter symmetry. Furthermore, magnetic excitations are also often considered as a possible glue for the Cooper-pairing in a number of heavy-fermion and transition metal oxides compounds.

An analysis of the feedback effect of superconductivity on the magnetic spin susceptibility can be used to determine the symmetry of the superconducting order parameter. This is of particular significance for recently discovered water intercalated sodium cobaltate superconductor[3], $Na_xCoO_2\cdot yH_2O$, where the origin of superconductivity as well as an underlying symmetry of the superconducting order parameter is currently under debate. The studies of the specific heat[4–7] and the μSR measurements of a magnetic penetration depth[8] have revealed a line of nodes in the superconducting gap function $\Delta_{\mathbf{k}}$. Similar conclusion has been made based on the measurements of the spin-lattice relaxation rate $1/T_1T$ by means of Nuclear Quadrupole Resonance (NQR), where absence of the characteristic Hebel-Slichter peak and power-law decrease upon decreasing temperature has been observed[9–13]. Simultaneously, the developing of the strong antiferromagnetic (AFM) fluctuations above superconducting transition temperature, T_c, have been found. At the same time, early reports on the Knight shift's temperature dependence, $K(T)$, have suggested a spin-triplet symmetry of the superconducting gap[14,15]. In these Nuclear Magnetic Resonance (NMR) experiments, $K(T)$ was shown to be anisotropic for external magnetic field applied parallel or perpendicular to the ab-plane. In particular, $K_c(T)$ component has not shown a substantial decrease below T_c. This behavior has been interpreted in favor of the odd-parity Cooper-pairing in sodium cobaltates[16–21]. However, the most recent NMR experiments with higher precision have found a reduction of both Knight shift components as a function of temperature for $T<T_c$[22,23]. These experiments points towards spin-singlet Cooper-pairing.

From the group-theoretical analysis the even-parity symmetries of the lowest harmonics for the triangular lattice are classified according to s-wave ($\Delta_{\mathbf{k}}=\Delta_0$), extended-$s$-wave ($\Delta_{\mathbf{k}}=2/3\Delta_0[\cos k_y+2\cos(k_x\sqrt{3}/2)\cos(k_y/2)]$), $d_{x^2-y^2}$-wave ($\Delta_{\mathbf{k}}=\Delta_0[\cos k_y-\cos(k_x\sqrt{3}/2)\cos(k_y/2)]$), d_{xy}-wave ($\Delta_{\mathbf{k}}=\Delta_0[\sqrt{3}\sin(k_x\sqrt{3}/2)\sin(k_y/2)]$), and $d_{x^2-y^2}+id_{xy}$-wave representations[24]. For both $d_{x^2-y^2}$-wave and d_{xy}-wave symmetries $\Delta_{\mathbf{k}}$ has line of nodes at the Fermi surface. Moreover, the time-reversal symmetry is broken for $d_{x^2-y^2}+id_{xy}$-wave state.

For the pure trigonal symmetry of the CoO_2-plane, all three d-wave states are degenerate. However, due to the absence of nodes $d_{x^2-y^2}+id_{xy}$-wave seems to be most energetically favorable. Until now, a breaking of time-reversal symmetry has not been observed in experiment[25,26]. Generally, the combined influence of the impurities and some competing instabilities, such as Cooper-pairing in a secondary channel as well as the lattice symmetry breaking, can lift the degeneracy be-

tween these three d-wave competing ground states[27]. This may indeed be the case for sodium cobaltates where Na arrangement introduces disorder at $x = 0.33$ concentration[28]. More sophisticated theories, involving multi-orbital model for sodium cobaltates, suggest two different gap symmetries (one of which is $d_{x^2-y^2} + id_{xy}$) for two different Fermi surface topologies[29].

Obviously, there is still a controversy on the symmetry of the superconducting order parameter in sodium cobaltates. In present study we systematically analyze the influence of the superconducting (SC) gap symmetry and the electronic structure on the dynamical spin susceptibility in $Na_xCoO_2{\cdot}yH_2O$. In particular, assuming spin singlet s-wave and d-wave symmetries of the superconducting order parameter we have calculated the real and the imaginary part of the magnetic response as a function of the momentum, temperature and frequency. We deduce the characteristic temperature dependencies of the Knight shift and spin-lattice relaxation rate. Furthermore, we have studied the feedback of the superconducting order parameter on the frequency dependence of the imaginary part of the spin susceptibility. We investigate the role played by the details of the electronic structure of $Na_xCoO_2{\cdot}yH_2O$ and, in particular, the changes of the Fermi surface (FS) topology induced by the multi-orbital effects.

Structurally, a parent compound, Na_xCoO_2, has a quasi-two-dimensional structure with Co ions in the CoO_2 layers forming a triangular lattice. Na ions reside between these layers and donate x electrons to the partially filled Co-$d(t_{2g})$ orbital. Apart from doping, Na ions also induce structural ordering at higher doping concentrations ($x \geq 0.5$) where superconductivity does not occur. Due to the presence of a trigonal crystalline electric field (CEF), the t_{2g} level splits into the higher lying a_{1g} singlet and the two lower lying e'_g states. The *ab-initio* band structure calculations within a Local Density Approximation (LDA) predict Na_xCoO_2 to have a large Fermi surface with mainly a_{1g} character and six hole pockets of mostly e'_g character[30]. At the same time, surface sensitive Angle-Resolved Photo-Emission Spectroscopy (ARPES)[31–33] reveals a doping dependent evolution of the Fermi surface, which shows no sign of the e'_g hole pockets for $0.3 \leq x \leq 0.8$. Instead, the observed Fermi surface is centered around the Γ point and has mostly a_{1g} character. It has been argued that such an effect may arise due to strong electronic correlations[34,35], however, no consensus in the literature has been reached yet (see e.g.[36–38]).

In $Na_xCoO_2{\cdot}yH_2O$ due to the water intercalation the inter-layer CoO_2 distance becomes larger and, thus, the trigonal CEF increases. Since the corresponding energy splitting between a_{1g} and e'_g levels is proportional to the trigonal crystal filed, it increases as well. For example, if one chooses a_{1g}-e'_g splitting $\delta\epsilon$ of about 150 meV, the six e'_g pockets disappear from the FS. Furthermore, upon water intercalation the material becomes more two-dimensional leading to a substantial decrease of the bi-layer splitting.

In order to take into account the multi-orbital effects we analyze the effect of superconductivity for the three different cases: the single-band (a_{1g}) model with nearest-neighbor hoppings, the realistic three-band (t_{2g}) model with, and without six e'_g pockets at the FS.

II. a_{1g}-BAND MODEL

We first consider the simple a_{1g}-band model, represented by a two-dimensional Hubbard Hamiltonian on the triangular lattice:

$$H = -\sum_{\mathbf{k},\sigma} \varepsilon_{\mathbf{k}} a^{\dagger}_{\mathbf{k}\sigma} a_{\mathbf{k}\sigma} + \sum_i U n_{i\uparrow} n_{i\downarrow}, \qquad (1)$$

where $n_{i\sigma} = a^{\dagger}_{i\sigma} a_{i\sigma}$, $a_{i\sigma}$ ($a^{\dagger}_{i\sigma}$) is the annihilation (creation) operator for the a_{1g} hole at the Co site i with spin σ. Here, $\varepsilon_{\mathbf{k}} = 2t[\cos k_y + 2\cos(k_x\sqrt{3}/2)\cos(k_y/2)] - \mu$, t=0.123 eV is the nearest-neighbor hopping integral, and μ is the chemical potential which has been calculated self-consistently for $x = 0.33$. The energy dispersion, $\varepsilon_{\mathbf{k}}$, along the principal directions of the hexagonal Brillouin zone (BZ) and the corresponding Fermi surface are shown in the inset of Fig. 1(a) and in the Fig. 1(b), respectively. Here, $\Gamma = (0,0)$, $\mathrm{K} = (0, 2/3)$, and $\mathrm{M} = (1/2\sqrt{3}, 1/2)$ [in units of $2\pi/a$] denote the symmetry points of the first BZ. Later, coordinates of the wave vectors will be given in units of $2\pi/a$ with a being the in-plane lattice constant.

To calculate the dynamical spin susceptibility, we employ the Random Phase Approximation (RPA) which gives

$$\chi_{RPA}(\mathbf{q}, i\omega_m) = \frac{\chi_0(\mathbf{q}, i\omega_m)}{1 - U\chi_0(\mathbf{q}, i\omega_m)}, \qquad (2)$$

where $\chi_0(\mathbf{q}, i\omega_m)$ is the BCS Lindhard susceptibility

$$\chi_0(\mathbf{q}, i\omega_m) = \frac{1}{2N}\sum_{\mathbf{k}} \Bigg[\frac{f(E_{\mathbf{k}+\mathbf{q}}) - f(E_{\mathbf{k}})}{i\omega_m - E_{\mathbf{k}+\mathbf{q}} + E_{\mathbf{k}}} C^{+}_{\mathbf{k},\mathbf{q}} + \frac{1 - f(E_{\mathbf{k}+\mathbf{q}}) - f(E_{\mathbf{k}})}{2} C^{-}_{\mathbf{k},\mathbf{q}} \times \left(\frac{1}{i\omega_m + E_{\mathbf{k}+\mathbf{q}} + E_{\mathbf{k}}} - \frac{1}{i\omega_m - E_{\mathbf{k}+\mathbf{q}} - E_{\mathbf{k}}} \right) \Bigg], \qquad (3)$$

with $C^{\pm}_{\mathbf{k},\mathbf{q}} = 1 \pm \frac{\varepsilon_{\mathbf{k}}\varepsilon_{\mathbf{k}+\mathbf{q}} + \mathrm{Re}(\Delta_{\mathbf{k}}\Delta^{*}_{\mathbf{k}+\mathbf{q}})}{E_{\mathbf{k}}E_{\mathbf{k}+\mathbf{q}}}$ being the BCS coherence factors. Here, ω_m are the Matsubara frequencies, $f(E)$ is the Fermi function, and $E_{\mathbf{k}} = \sqrt{\varepsilon_{\mathbf{k}} + |\Delta_{\mathbf{k}}|^2}$.

In Fig. 1(a) we show both the bare and the RPA magnetic susceptibility in the normal state at $\omega = 5$ meV and $U = 0.25$ eV. One immediately notices that the magnetic response is dominated by the scattering at the *incommensurate* wave vector, $\mathbf{Q_{SDW}} = (0, 0.598) \approx (0, 3/5)$. The value of $\mathrm{Im}[\chi(\mathbf{q}, \omega)]$ at the commensurate wave vector, $\mathbf{Q_{AFM}} = (0, 2/3)$, appears to be much smaller. There

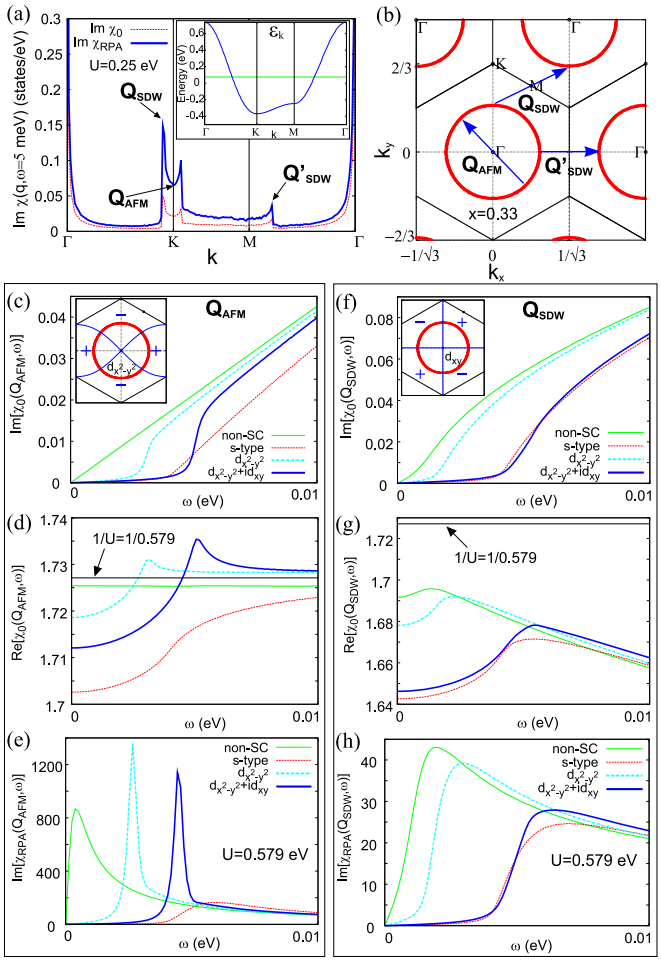

FIG. 1: (Color online) Calculated results for the a_{1g}-band model. (a) $\mathbf{q}$-dependence of $\mathrm{Im}[\chi_0(\mathbf{q},\omega)]$ and $\mathrm{Im}[\chi_{RPA}(\mathbf{q},\omega)]$ at $\omega = 5$ meV in the normal (non-SC) phase. The scattering wave vectors $\mathbf{Q_{AFM}}$, $\mathbf{Q_{SDW}}$, and $\mathbf{Q'_{SDW}}$ are denoted by the arrows. In the inset the a_{1g}-band dispersion is shown, where the horizontal (green) line stands for the chemical potential. (b) The calculated Fermi surface with the corresponding scattering wave vectors. The panels (c)-(e) show imaginary and real parts of χ_0, and imaginary part of χ_{RPA} at $\mathbf{q} = \mathbf{Q_{AFM}}$ in non-SC phase and in SC phase with various superconducting order parameter symmetries. The same quantities are plotted in the panels (f)-(h) at the wave vector $\mathbf{q} = \mathbf{Q_{SDW}}$. The nodes of the $d_{x^2-y^2}$-wave and d_{xy}-wave superconducting gaps in the first BZ are shown in the insets of (c) and (f), respectively. Here we choose the amplitude of the superconducting order parameter $\Delta_0 = 2$ meV. For the numerical purposes we also employ the broadening of the Green's function, $\delta = 0.2$ meV.

is also another incommensurate wave vector present, $\mathbf{Q'_{SDW}}$. Both $\mathbf{Q_{SDW}}$ and $\mathbf{Q'_{SDW}}$ correspond to the umklapp processes, as it is seen from the FS plot in Fig. 1(b). The presence of a set of incommensurate wave vectors with substantial magnitude of magnetic scattering shows a tendency of the itinerant electrons on the triangular lattice towards spin density wave (SDW) instability.

In Fig. 1(c) and (d) we present the imaginary and the

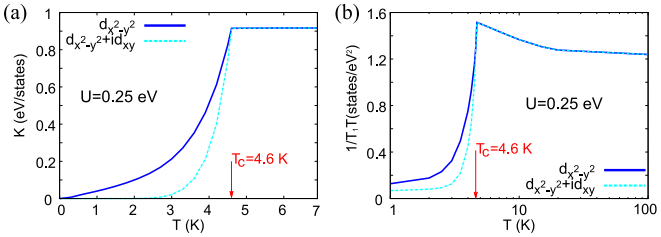

FIG. 2: Calculated temperature dependence of the Knight shift $K(T)$ (a) and the spin-lattice relaxation rate $1/T_1T$ (b) for the a_{1g}-band model. Note the logarithmic temperature scale in (b). Here, we assume the conventional BCS temperature dependence of superconducting gap, $\Delta_0(T) = \Delta_0\sqrt{1-T/T_c}$.

real parts of $\chi_0(\mathbf{Q_{AFM}},\omega)$ as a function of frequency ω at $T = 1$ K. In the non-SC state, the imaginary part is linear in ω at low frequencies which is a typical Landau damping within the Fermi-liquid picture. In the SC phase, the imaginary part of the magnetic susceptibility becomes gapped. The magnitude of the gap, Ω_g, is equal to $2\Delta_0$ in the s-wave case. At larger frequencies $\mathrm{Im}\chi_0$ increases slowly from zero. In comparison, for the d-wave symmetries the value $\Omega_g = |\Delta_{\mathbf{k}}| + |\Delta_{\mathbf{k}+\mathbf{Q}}|$ is smaller than $2\Delta_0$. Furthermore, as it is readily seen from the insets of Fig. 1(c) and (f), $\Delta_{\mathbf{k}} = -\Delta_{\mathbf{k}+\mathbf{Q_{AFM}}}$ at the FS which yields a discontinuous jump of $\mathrm{Im}\chi_0$ at Ω_g. Correspondingly, the real part will possess a logarithmic singularity as it is also shown in Fig. 1(d). Within the RPA the formation of the pole (spin resonance) in the total magnetic susceptibility below Ω_g is possible if $\mathrm{Im}[\chi_0(\mathbf{q},\omega)] = 0$ and simultaneously $1/U = \mathrm{Re}[\chi_0(\mathbf{q},\omega)]$. Due to the logarithmic character of the singularity this condition will be generally fulfilled for any small value of U which would give a position of the resonance exactly at or very close to Ω_g. However, a small amount of impurities or disorder will smear the singularity out and suppress the resonance peak. In $Na_xCoO_2{\cdot}yH_2O$ the value of U should be relatively large which shifts the position of the spin resonance towards energies smaller than Ω_g and makes it robust against impurity scattering. The calculated susceptibility is shown in Fig. 1(e) where we use U_{res}=0.579 eV. It is interesting to note that the resonance occurs for both $d_{x^2-y^2}$- and $d_{x^2-y^2} + id_{xy}$-wave symmetries, however, for different values of Ω_g. The present value of U_{res} is of course too small to be the on-site Coulomb repulsion which is of the order of several electron volts. Therefore, the effective interaction U entering our model (1) originates mainly from the Hund's exchange, J_H. In the lamellar sodium cobaltate, the value of J_H is about 1 eV[39]. Taking this value into account, one assumes $U = \alpha J_H$, where J_H is the mean-field value of the Hund's exchange and α is the coefficient that describes corrections beyond mean-field theory.

The situation changes for the wave vector $\mathbf{Q_{SDW}}$ [Fig. 1(f)-(h)]. There is one striking difference in the low-energy behavior of $\mathrm{Im}[\chi_0(\mathbf{Q_{SDW}},\omega)]$. Namely, already in

the normal state the scattering rate is *non-linear* for small ω. It is obviously a consequence of the $2\mathbf{k_F}$ instability and a resulting non-Landau damping at this wave vector. Furthermore, in the SC state the SDW wave vector connects now states with the same sign of the superconducting order parameter. As a result the discontinuity does not occur and the real part of χ_0 is always smaller in the superconducting state than in the normal state. Therefore, for reasonable values of U there is no resonance condition for χ_{RPA} [see Fig. 1(h)].

Generally, a formation of the resonance peak below T_c in the unconventional superconductors is a well-known consequence of the sign change of the superconducting order parameter. It has been originally discussed in relation to the layered high-T_c cuprates[40] and also recently has been used to explain the inelastic neutron scattering results in heavy-fermion compound UPd_2Al_3[41]. In layered superconducting cobaltates the emergence of the resonance peak for several symmetries of the superconducting order parameter has been analyzed within simple single-band model[42]. In contrast to Ref. 42, we have found that the resonance peak (even within simple a_{1g}-band model) is very sensitive to the small variation of U-values and to disorder. As a result the resonance is confined to the wave vector $\mathbf{Q_{AFM}}$ and disappears for $|\mathbf{Q}| < |\mathbf{Q_{AFM}}|$.

The temperature dependence of the Knight shift, $K(T)$, and the spin-lattice relaxation rate, $1/T_1T$, is calculated according to the expressions:

$$K(T) \propto \lim_{\mathbf{q}\to 0} \mathrm{Re}\chi(\mathbf{q},\omega=0), \qquad (4)$$

$$1/T_1T \propto \lim_{\omega\to 0} \frac{1}{\pi}\sum_{\mathbf{q}} \frac{\mathrm{Im}\chi(\mathbf{q},\omega)}{\omega}. \qquad (5)$$

In Fig. 2 we show both quantities as a function of temperature. In the normal state $1/T_1T$ increases with decreasing temperature that reflects the presence of the incommensurate antiferromagnetic fluctuations in this system. At the same time, the Knight shift is a constant which stresses that there are no small-$\mathbf{q}$ fluctuations. Below T_c both physical observables drop rapidly due to opening of the superconducting gap in the energy spectrum. As expected, the decrease is exponential for $d_{x^2-y^2}+id_{xy}$-wave symmetry due to its nodeless character in $E_{\mathbf{k}}$. For $d_{x^2-y^2}$-wave symmetry the behavior of $1/T_1T$ and $K(T)$ follows standard power-law temperature dependence due to the presence of the line nodes in the energy spectrum. In the next section we will compare our results to the experimental data where we describe a more realistic model in application to the superconducting cobaltate.

III. t_{2g}-BAND MODEL

The a_{1g}-band model is, of course, oversimplified for describing the physics of $Na_xCoO_2{\cdot}yH_2O$ since a_{1g}-e'_g level splitting, $\delta\epsilon$, is only 53 meV. As a result there is a substantial hybridization of the a_{1g} and the e'_g bands, completely neglected in the simple a_{1g}-band model. In particular, the e'_g bands may form hole pockets at the FS in addition to a large a_{1g}-pocket[30]. To take into account these details, we further analyze the magnetic response in the full t_{2g}-band model including both a_{1g} and e'_g cobalt states.

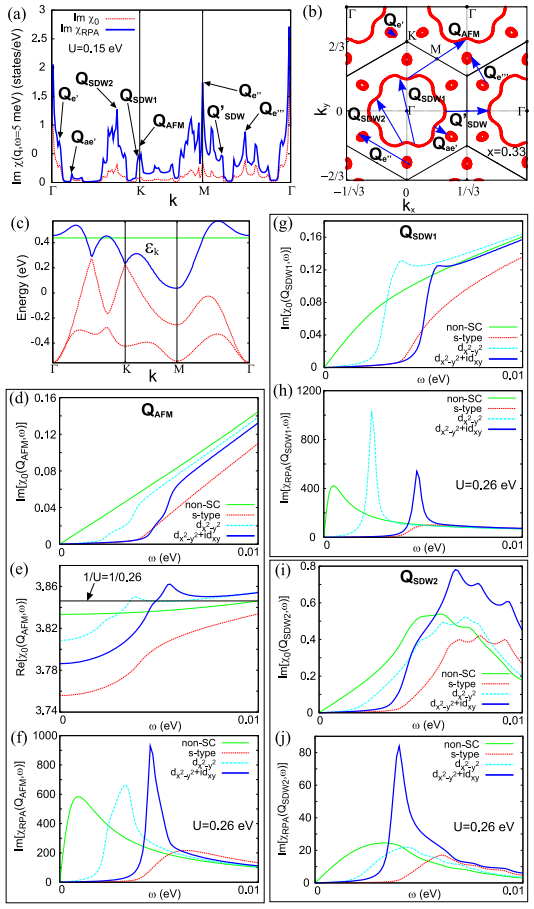

FIG. 3: (Color online) Calculated results for the t_{2g}-band model. (a) $\mathbf{q}$-dependence of $\mathrm{Im}[\chi_0(\mathbf{q},\omega)]$ and $\mathrm{Im}[\chi_{RPA}(\mathbf{q},\omega)]$ at $\omega = 5$ meV in the normal (non-SC) phase. The scattering wave vectors $\mathbf{Q_{AFM}}$, $\mathbf{Q_{SDW1}}$, $\mathbf{Q_{SDW2}}$, $\mathbf{Q'_{SDW}}$, $\mathbf{Q_{ae'}}$, $\mathbf{Q_{e'}}$, $\mathbf{Q_{e''}}$, and $\mathbf{Q_{e'''}}$ are denoted by the arrows. (b) The calculated Fermi surface with the corresponding scattering wave vectors. In (c) the band dispersion is shown where the bold (blue) curve denotes the topmost band used for the susceptibility calculations. A horizontal (green) line stands for the chemical potential. The panels (d)-(f) show imaginary and real parts of χ_0, and imaginary part of χ_{RPA} at $\mathbf{q} = \mathbf{Q_{AFM}}$ in the normal state and in SC state with various superconducting order parameter symmetries. The imaginary parts of the bare and the total susceptibilities are plotted in the panels (g)-(h) and (i)-(j) at the wave vectors $\mathbf{q} = \mathbf{Q_{SDW1}}$ and $\mathbf{q} = \mathbf{Q_{SDW1}}$, respectively. Here we choose the amplitude of the superconducting order parameter $\Delta_0 = 2$ meV. For the numerical purposes we also employ the broadening of the Green's function, $\delta = 0.2$ meV.

The free electron Hamiltonian of the t_{2g}-band model

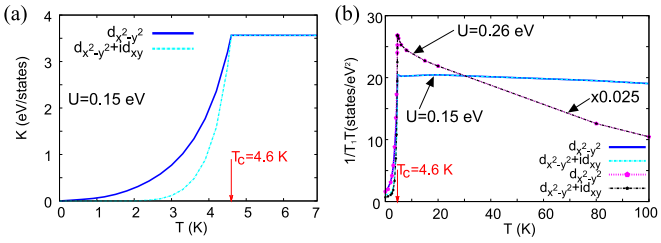

FIG. 4: Calculated temperature dependence of the Knight shift $K(T)$ (a) and the spin-lattice relaxation rate $1/T_1T$ (b) for the t_{2g}-band model.

in a hole representation is given by

$$H_0 = -\sum_{\mathbf{k},\alpha,\sigma} (\epsilon^{\alpha} - \mu)\, n_{\mathbf{k}\alpha\sigma} - \sum_{\mathbf{k},\sigma} \sum_{\alpha,\beta} t_{\mathbf{k}}^{\alpha\beta} d_{\mathbf{k}\alpha\sigma}^{\dagger} d_{\mathbf{k}\beta\sigma}, \quad (6)$$

where $n_{\mathbf{k}\alpha\sigma} = d_{\mathbf{k}\alpha\sigma}^{\dagger} d_{\mathbf{k}\alpha\sigma}$, $d_{\mathbf{k}\alpha\sigma}$ ($d_{\mathbf{k}\alpha\sigma}^{\dagger}$) is the annihilation (creation) operator for the t_{2g}-hole with spin σ, orbital index α, and momentum $\mathbf{k}$, $t_{\mathbf{k}}^{\alpha\beta}$ is the hopping matrix element, ϵ^{α} is the single-electron energy, and μ is the chemical potential. All of the in-plane hoppings and the single-electron energies were derived previously by us from the *ab-initio* LDA calculations, and we use here the parameters for x=0.33 from Ref. 35. To obtain the dispersion we diagonalize the Hamiltonian (6) calculating the chemical potential μ self-consistently. The resulting FS topology and energy dispersion are shown in Fig. 3(b) and (c), respectively.

Due to the non-zero inter-orbital hopping matrix elements, a_{1g} and e_g' bands are hybridized. However, only one of the hybridized bands crosses the Fermi level thus making the largest contribution to the low-energy properties of the system. We refer to this band as $\varepsilon_{\mathbf{k}}$. Note, it is substantially different from the simple a_{1g}-band. Later, this effective band $\varepsilon_{\mathbf{k}}$ will be used to calculate the dynamical magnetic susceptibility with some effective on-site Coulomb interaction U.

Present FS has more complicated structure in comparison to the a_{1g}-band model. This results in a number of additional scattering wave vectors as calculated from χ_0, see Fig. 3(a). In particular, there are three wave vectors that are solely due to the e_g' FS pockets ($\mathbf{Q_{e'}}$, $\mathbf{Q_{e''}}$, and $\mathbf{Q_{e'''}}$), the one wave vector is due to a_{1g}-e_g' scattering ($\mathbf{Q_{ae'}}$), and the two other wave vectors are due to the curved form of the central a_{1g} FS pocket ($\mathbf{Q_{SDW1}} = (0, 0.649)$ and $\mathbf{Q_{SDW2}} = (0, 0.495)$). The pronounced peaks at all these wave vectors are present in both the bare and the RPA magnetic susceptibility (U=0.15 eV). Again, similar to the a_{1g}-band model, the magnetic response is not dominated by the scattering at the commensurate wave vector $\mathbf{Q_{AFM}}$. The overall picture of the magnetic response is consistent with the one presented in Ref. 19.

In the non-SC phase and the SC phase with s-wave order parameter the behavior of $\chi(\mathbf{q},\omega)$ at $\mathbf{q} = \mathbf{Q_{AFM}}$ [see Fig. 3(d)-(f)] is similar to the one in the a_{1g}-band model. However, for the d-wave symmetry of the order parameter, one finds that for $\omega \geq \Omega_g$ the states with equal signs of the superconducting order parameter contributes first, and the discontinuous jump in $\mathrm{Im}[\chi_0(\mathbf{Q_{AFM}},\omega)]$ occurs at higher energies. The particular form of the FS in the realistic t_{2g}-band model and more complicated band structure produce this effect. Therefore, the resonance peak in $\mathrm{Im}[\chi_{RPA}(\mathbf{Q_{AFM}},\omega)]$ may in principle still exist, however, it occurs in a very narrow interval of the U values. This interval is determined by the resonance condition in the superconducting state and by the stability of a paramagnetic state above T_c. Here, we use U_{res}=0.26 eV, which is more than twice smaller than in the a_{1g}-band model.

Although the formation of the spin resonance is unrealistic for the antiferromagnetic wave vector $\mathbf{Q_{AFM}}$ it may now occur at other wave vectors. In Fig. 3(g)-(j) we present the imaginary parts of $\chi_0(\mathbf{q},\omega)$ and $\chi_{RPA}(\mathbf{q},\omega)$ at $\mathbf{Q_{SDW1}}$ and at $\mathbf{Q_{SDW2}}$. Here, one notices the pronounced effects of the complicated t_{2g}-band structure at high energies for the scattering at both wave vectors. Deviations from the linear-ω damping start already at low energies, smaller than Ω_g. For $U = U_{res}$ the spin-resonance is present at $\mathbf{Q_{SDW1}}$ for both d-wave symmetries. However, at $\mathbf{Q_{SDW2}}$ the resonance peak is present for $d_{x^2-y^2} + id_{xy}$-wave symmetry only. Similar to the situation with $\mathbf{Q_{AFM}}$, this is due to smallness of the allowed U values.

In Fig. 4 we show the corresponding results for the $1/T_1T$ and $K(T)$. Below superconducting transition temperature the behavior is very similar to the results obtained for the simple a_{1g}-band model. This is because below T_c the symmetry of the superconducting gap and its nodal structure determines the temperature dependencies of the $1/T_1T$ and the $K(T)$ values. At the same time, notice the stronger AFM fluctuations in the normal state. For almost the same value of U this is due to the narrower conduction band than in the simple a_{1g}-band model. Such a behavior is observed in the experimental NQR data[9,11,43]. It is interesting to note that without water the parent non-superconducting compound $Na_{0.33}CoO_2$ shows much weaker AFM fluctuations[11]. In our theory the fluctuations occur for the parent compound too. It probably demonstrates a possible significance of the third dimension and, in particular, the bilayer splitting which may reduce the two-dimensional AFM fluctuations in $Na_{0.33}CoO_2$.

Note, the presence of the e_g' pockets on the FS can also lift the degeneracy between the three d-wave states. Since in the $d_{x^2-y^2}$-wave SC state the e_g' FS pockets are fully gapped, the additional condensation energy is gained [compare the topology of the line-nodes in the inset in Fig. 1(c) and FS topology in Fig. 3(b)]. For the d_{xy}-wave SC state this gain in energy will be smaller [compare the inset in Fig. 1(f) and FS in Fig. 3(b)].

Presently, there is still a discussion on the details of the Fermi surface topology in the water intercalated cobaltates. In particular, ARPES experiments do not ob-

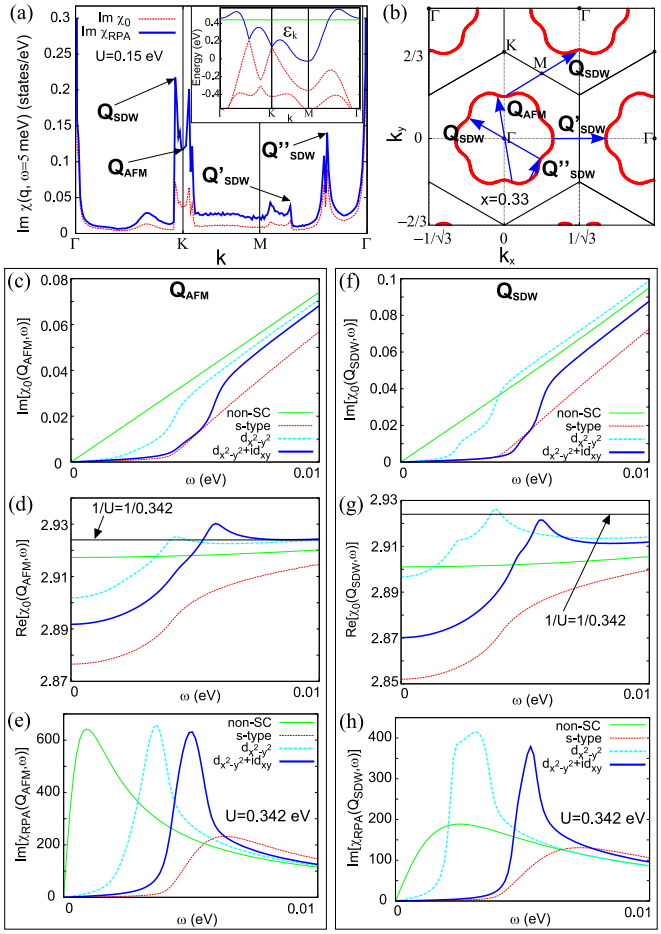

FIG. 5: (Color online) Calculated results for the t_{2g}-band model with enlarged crystal field splitting. (a) $\mathbf{q}$-dependence of the $\mathrm{Im}[\chi_0(\mathbf{q},\omega)]$ and the $\mathrm{Im}[\chi_{RPA}(\mathbf{q},\omega)]$ at $\omega = 5$ meV in the normal (non-SC) phase. The scattering wave vectors $\mathbf{Q_{AFM}}$, $\mathbf{Q_{SDW}}$, $\mathbf{Q'_{SDW}}$, and $\mathbf{Q''_{SDW}}$ are denoted by the arrows. The band dispersion is shown in the inset of (a), where the bold (blue) curve denotes the topmost band used for the susceptibility calculations, and the horizontal (green) line stands for the chemical potential. (b) The calculated Fermi surface with the corresponding scattering wave vectors. (c)-(e) The calculated imaginary (c) and real (d) parts of the $\chi_0(\mathbf{Q_{AFM}},\omega)$, and the imaginary part of χ_{RPA} (e) in the normal and in the SC state with various superconducting order parameters. The same quantities are plotted in (f)-(h) at $\mathbf{q} = \mathbf{Q_{SDW}}$. Here we choose the amplitude of the superconducting order parameter $\Delta_0 = 2$ meV. For the numerical purposes we also employ the broadening of the Green's function, $\delta = 0.2$ meV.

serve the e'_g-pockets at the FS[31–33]. It has been shown that an inclusion of the electronic correlation within Gutzwiller approximation may shift the e'_g-bands below the Fermi level[34,35], although this conclusion has been challenged[36–38]. In our study we further consider the t_{2g}-band model with increased crystal filed splitting, $\delta\epsilon$=153 meV. This makes e'_g band sink below the Fermi level, as it is seen in the inset of Fig. 5(a). The behavior of the

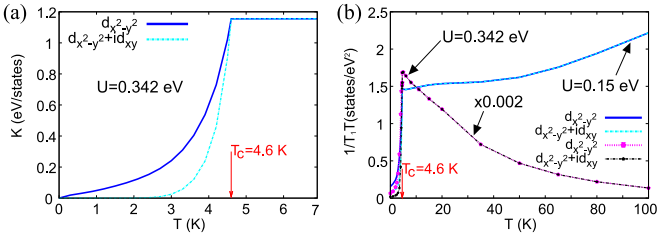

FIG. 6: (Color online) Calculated temperature dependence of the Knight shift $K(T)$ (a) and the spin-lattice relaxation rate $1/T_1T$ (b) for the t_{2g}-band model without e'_g FS pockets.

dynamical spin susceptibility for U=0.15 eV at $\omega = 5$ meV presented in Fig. 5(a) shows more similarity to the simple a_{1g}-band model with additional features due to peculiarities ("rounded hexagon" form) of the large FS pocket as shown in Fig. 5(b). The scattering is most pronounced at the wave vector $\mathbf{Q_{SDW}} = (0, 0.633)$, which is smaller than in the simple a_{1g}-band model. There is also intensive scattering at the wave vector $\mathbf{Q''_{SDW}}$, owing its appearance to the curved shape of the FS.

Fig. 5(c)-(e) and (f)-(h) displays the magnetic susceptibility at $\mathbf{Q_{AFM}}$ and at $\mathbf{Q_{SDW}}$, respectively. Contrary to both a_{1g}-band model and t_{2g}-band model with e'_g FS pockets, here we observe a well-defined linear behavior of $\mathrm{Im}[\chi_0(\mathbf{q},\omega)]$ in the considered frequency range at these wave vectors. For the d-wave order parameter, the behavior of the susceptibility resembles that in the t_{2g}-band model with e'_g FS pockets. Again one could find a narrow range of parameters where the resonance peak exists, which we illustrate in Fig. 5(e),(h) for U_{res}=0.342 eV.

Similarly, the change of the FS topology does not influence significantly the temperature dependence of the Knight shift and the spin-lattice relaxation rate above and below T_c. This is illustrated in Fig. 6 where we plot both quantities as a function of temperature.

IV. CONCLUSION

Our analysis of the dynamical spin susceptibility in application to the $Na_xCoO_2{\cdot}yH_2O$ have shown that the magnetic response in the normal state is dominated by the incommensurate SDW fluctuations at large momenta close to $\mathbf{Q_{AFM}}$. This is consistent with experimental NQR data which shows a pronounced AFM-like fluctuations in the temperature dependence of the spin-lattice relaxation rate. It is interesting to note that the presence of the e'_g-pockets at the Fermi surface is not affecting significantly this result. In the normal state we note the absence of ferromagnetic-like fluctuations. This observation justifies our choice of spin-singlet order parameter, because to induce the spin-triplet Cooper-pairing the fluctuations with small momenta are required. Below T_c our results for $d_{x^2-y^2}$- or d_{xy}-wave (not shown) symmetries of the superconducting order parameter are consistent with experimental data which excludes node-

less $d_{x^2-y^2}+id_{xy}$-wave symmetry. We further stress that the resonance peak, predicted previously[42] for the simple a_{1g}-band model, is improbable for the realistic band structure of $Na_xCoO_2{\cdot}yH_2O$. Moreover, we find that even if present the resonance peak is confined to the AFM wave vector and disappears away from it.

Acknowledgments

We would like to thank A. Donkov, V. Yushankhai, and G.-p. Zheng for useful discussions, and I. Mazin for useful comments. M.M.K. acknowledge support form INTAS (YS Grant 05-109-4891) and RFBR (Grants 06-02-16100, 06-02-90537-BNTS). I.E. acknowledge support form Volkswagen Foundation.

* Electronic address: maxim@mpipks-dresden.mpg.de

[1] D. Vollhardt and P. Woelfle, *The Superfluid Phases of Helium 3* (Taylor and Francis, London, 1990).
[2] see H.F. Fong, P. Bourges, Y. Sidis, L.P. Regnault, J. Bossy, A. Ivanov, D.L. Milius, I.A. Aksay, and B. Keimer, Phys. Rev. B **61**, 14773 (2000) and references therein.
[3] K. Takada, H. Sakurai, E. Takayama-Muromachi, F. Izumi, R.A. Dilanian, and T. Sasaki, Nature **422**, 53 (2003).
[4] G. Cao, C. Feng, Y. Xu, W. Lu, J. Shen, M. Fang, and Z.-a. Xu, J. Phys.: Condens. Matter **15**, L519 (2003).
[5] B. Lorenz, J. Cmaidalka, R.L. Meng, and C.W. Chu, Physica C **402**, 106 (2004).
[6] H.D. Yang, J.-Y. Lin, C.P. Sun, Y.C. Kang, C.L. Huang, K. Takada, T. Sasaki, H. Sakurai, and E. Takayama-Muromachi, Phys. Rev. B. **71**, 020504(R) (2005).
[7] R. Jin, B.C. Sales, S. Li, and D. Mandrus, Phys. Rev. B **72**, 060512(R) (2005).
[8] A. Kanigel, A. Keren, L. Patlagan, K.B. Chashka, P. King, and A. Amato, Phys. Rev. Lett **92**, 257007 (2004).
[9] T. Fujimoto, G.-q. Zheng, Y. Kitaoka, R.L. Meng, J. Cmaidalka, and C.W. Chu, Phys. Rev. Lett. **92**, 047004 (2004).
[10] K. Ishida, Y. Ihara, K. Kitagawa, H. Murakawa, Y. Maeno, C. Michioka, M. Kato, K. Yoshimura, K. Takada, T. Sasaki, H. Sakurai, and E. Takayama-Muromachi, J. Phys. Soc. Jpn. **72**, 3041 (2003).
[11] G.-q. Zheng, K. Matano, R.L. Meng, J. Cmaidalka, and C.W. Chu, J. Phys.: Condens. Matter **18**, L63 (2006).
[12] Y. Ihara, H. Takeya, K. Ishida, H. Ikeda, C. Michioka, K. Yoshimura, K. Takada, T. Sasaki, H. Sakurai, and E. Takayama-Muromachi, J. Phys. Soc. Jpn. **75**, 124714 (2006).
[13] C. Michioka, H. Ohta, Y. Itoh, and K. Yoshimura, J. Phys. Soc. Jpn. **75**, 063701 (2006).
[14] M. Kato, C. Michioka, T. Waki, K. Yoshimura, K. Ishida, H. Sakurai, E. Takayama-Muromachi, K. Takada, T. Sasaki, Physica B **359-361**, 482 (2005).
[15] Y. Ihara, K. Ishida, H. Takeya, C. Michioka, M. Kato, Y. Itoh, K. Yoshimura, K. Takada, T. Sasaki, H. Sakurai, and E. Takayama-Muromachi, J. Phys. Soc. Jpn. **75**, 013708 (2006).
[16] A. Tanaka and X. Hu, Phys. Rev. Lett. **91**, 257006 (2003).
[17] O.I. Motrunich and P.A. Lee, Phys. Rev. B **70**, 024514 (2004).
[18] K. Kuroki, Y. Tanaka, and R. Arita, Phys. Rev. Lett. **93**, 077001 (2004).
[19] M.D. Johannes, I.I. Mazin, D.J. Singh, and D.A. Papaconstantopoulos, Phys. Rev. Lett. **93**, 097005 (2004).
[20] K. Kuroki, Y. Tanaka, and R. Arita, Phys. Rev. B **71**, 024506 (2005).
[21] M. Mochizuki, Y. Yanase, and M. Ogata, Phys. Rev. Lett. **94**, 147005 (2005).
[22] G.-q. Zheng, K. Matano, D.P. Chen, and C.T. Lin, Phys. Rev. B **73**, 180503(R) (2006).
[23] Y. Kobayashi, T. Moyoshi, H. Watanabe, M. Yokoi, and M. Sato, J. Phys. Soc. Jpn. **75**, 074717 (2006).
[24] see I.I. Mazin and M.D. Johannes, Nature physics **1**, 91 (2005) and references therein.
[25] W. Higemoto, K. Ohishi, A. Koda, S.R. Saha, R. Kadono, K. Ishida, K. Takada, H. Sakurai, E. Takayama-Muromachi, and T. Sasaki, Phys. Rev. B **70**, 134508 (2004).
[26] W. Higemoto, K. Ohishi, A. Koda, R. Kadono, H. Sakurai, K. Takada, E. Takayama-Muromachic, and T. Sasaki, Physica B **374**, 274 (2006).
[27] S. Florens and M. Vojta, Phys. Rev. B **71**, 094516 (2005).
[28] H.W. Zandbergen, M. Foo, Q. Xu, V. Kumar, and R.J. Cava, Phys. Rev. B **70**, 024101 (2004).
[29] M. Mochizuki and M. Ogata, J. Phys. Soc. Jpn. **76**, 013704 (2007).
[30] D.J. Singh, Phys. Rev. B **61**, 13397 (2000).
[31] M.Z. Hasan, Y.-D. Chuang, D. Qian, Y.W. Li, Y. Kong, A. Kuprin, A.V. Fedorov, R. Kimmerling, E. Rotenberg, K. Rossnagel, Z. Hussain, H. Koh, N.S. Rogado, M.L. Foo, and R.J. Cava, Phys. Rev. Lett. **92**, 246402 (2004).
[32] H.-B. Yang, S.-C. Wang, A.K.P. Sekharan, H. Matsui, S. Souma, T. Sato, T. Takahashi, T. Takeuchi, J.C. Campuzano, R. Jin, B.C. Sales, D. Mandrus, Z. Wang, and H. Ding, Phys. Rev. Lett. **92**, 246403 (2004).
[33] T. Shimojima, K. Ishizaka, S. Tsuda, T. Kiss, T. Yokoya, A. Chainani, S. Shin, P. Badica, K. Yamada, and K. Togano, Phys. Rev. Lett. **97**, 267003 (2006).
[34] S. Zhou, M. Gao, H. Ding, P.A. Lee, and Z. Wang, Phys. Rev. Lett. **94**, 206401 (2005).
[35] M.M. Korshunov, I. Eremin, A. Shorikov, V.I. Anisimov, M. Renner, and W. Brenig, Phys. Rev. B **75**, 094511 (2007).
[36] H. Ishida, M.D. Johannes, and A. Liebsch, Phys. Rev. Lett. **94**, 196401 (2005).
[37] C. A. Perroni, H. Ishida, and A. Liebsch, Phys. Rev. B **75**, 045125 (2007).

[38] A. Liebsch and H. Ishida, cond-mat/0705.3627 (unpublished).
[39] A.O. Shorikov, V.I. Anisimov, and M.M. Korshunov, cond-mat/0705.1408 (unpublished).
[40] see I. Eremin, D.K. Morr, A.V. Chubukov, K.H. Bennemann, and M.R. Norman, Phys. Rev. Lett. **94**, 147001 (2005) and references therein.
[41] J. Chang, I. Eremin, P. Thalmeier, and P. Fulde, Phys. Rev. B **75**, 024503 (2007).
[42] J.-X. Li and Z.D. Wang, Phys. Rev. B **70**, 212512 (2004).
[43] Y. Ihara, K. Ishida, K. Yoshimura, K. Takada, T. Sasaki, H. Sakurai, and E. Takayama-Muromachi, J. Phys. Soc. Jpn. **74**, 2177 (2005).